Soft Matter

Tiny plastic, big trouble: how polystyrene nanoparticles impact DNA-damage repair deficient cervical cancer cells

Jordan D. Berezowitz, [ID] [ab] Mira C. Fish,[acd] Lauren E. Mehanna,[ae] Breanna Knicely,[f] Claire E. Rowlands,[a] Eva M. Goellner[fg] and Brittany E. Givens [ID] *[a]

Microplastics are becoming increasingly abundant waste products; therefore, the risk of human exposure is also increasing. The cytotoxic consequences of microplastic exposure, particularly in cancer, have yet to be explored. We obtained commercially available polystyrene nanoparticles of uniform size (86.61 ± 6.41 nm) and confirmed the chemical composition and shape using Fourier transform infrared spectroscopy (FTIR) and scanning electron microscopy (SEM), respectively. We evaluated colloidal stability over a range of concentrations from 1–1000 µg mL^{-1} using hydrodynamic diameter and zeta potential, determining that higher concentrations exhibit greater colloidal stability compared to lower concentrations. Specifically, the zeta potential increased from very negative values of approximately −40 mV to approximately zero mV. To evaluate the cytotoxic effects of these microplastics, we evaluated the relative cell viability *in vitro* of HeLa cervical cancer cells, including those with DNA damage repair deficiencies in MLH1 and MSH2. High concentrations of polystyrene were required for observable decreases in cell viability, particularly in esterase activity measured with calcein AM. Cellular internalization of the nanoparticles was confirmed quantitatively using intracellular fluorescence and qualitatively using confocal microscopy for fluorescent polystyrene. Overall, these results indicate that high concentrations of polystyrene are required to elicit toxicological effects in cervical cells within 24 hours.

Introduction

By 2050, it is projected that 26 billion tons of plastic waste will be generated worldwide.[1] Since the 1950s, plastic use has been nearly ubiquitous in virtually every field and industry.[2,3] However, the degradation and subsequent contamination of environmental sources as micro- and nano-plastic materials went unnoticed for decades. Approximately 75% of plastic is improperly recycled, thus contributing to the accumulation of plastic waste in water, soil, and air. Nanoplastics and microplastics have been identified as degradation products from a

breadth of consumer products, including but not limited to: tires and brakes,[4,5] water bottles,[6,7] clothing,[8] and feminine hygiene products.[9,10] The European Water Framework Directive defines "microplastics" as particles in the size range of 1–5 mm and "small microplastics" as those in the size range of 25 µm–1 mm.[11] This term was first coined by Richard Thompson in 2004.[12] Although these particles can be in the millimetre range, the "micro" prefix refers to the small nature of particles rather than a metric prefix.[11] Microplastics can further break down into nanoplastics with sizes <1 µm or 100 nm, depending on the definition that is used.[2] These smaller particles can then proceed to contaminate food sources, such as fish, or drinking water (Fig. 1).[13]

Exposure to these plastics may cause hormone dysfunction, classifying them as endocrine-disrupting chemicals (EDCs), which are chemicals from outside the body that interfere with the endocrine system, including oestrogen and progesterone-responsive gynaecological tissues.[14] Nanoplastics exhibit higher colloidal stability and mobility and have a higher uptake potential due to their small size, thus making them dangerous for human cells if accumulation occurs.[2,3] One such amorphous nanoplastic, polystyrene (PS),[15] has been shown to impact brain development for exposure during the perinatal

[a] *Department of Chemical and Materials Engineering, Stanley and Karen Pigman College of Engineering, University of Kentucky, Lexington, USA. E-mail: brittany.givens@uky.edu*

[b] *School of Chemical and Biomolecular Engineering, Georgia Institute of Technology, Atlanta, GA, USA*

[c] *Department of Biology, Brandeis University, Waltham, MA, USA*

[d] *Integrated Biomedical Sciences Program, College of Medicine, University of Kentucky, Lexington, USA*

[e] *Programs of Chemistry and Engineering, Centre College, Danville, KY, USA*

[f] *Department of Toxicology and Cancer Biology, College of Medicine, University of Kentucky, Lexington, USA*

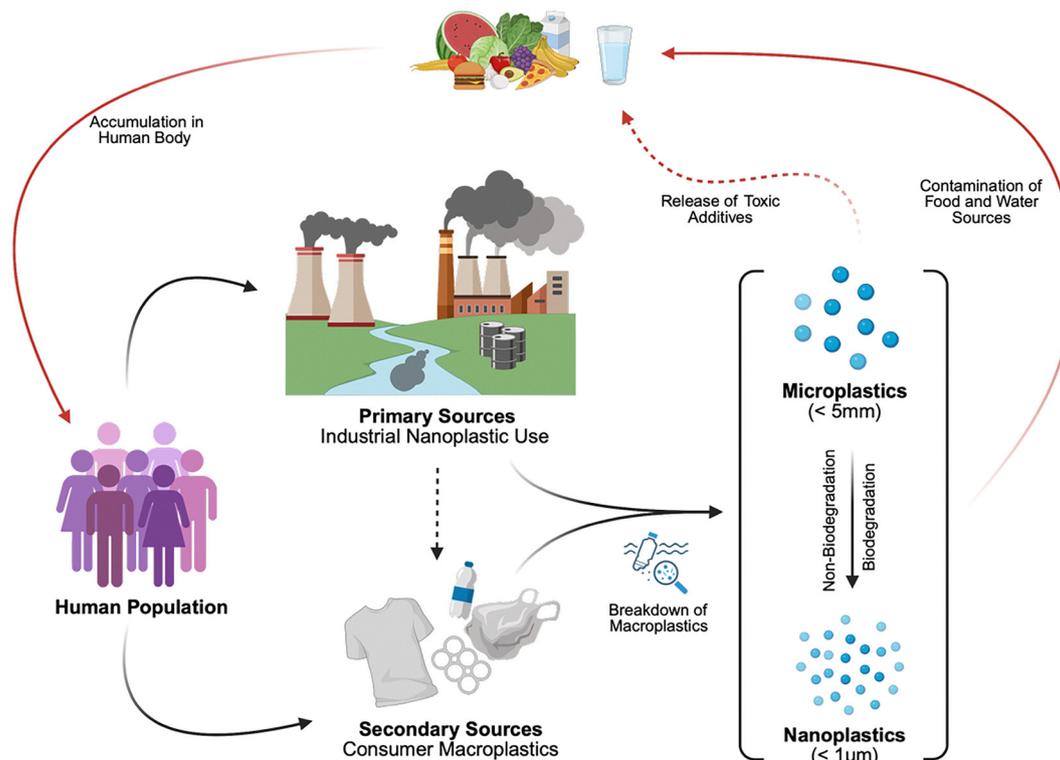[g] *Department of Biology, Georgetown College, Georgetown, KY, USA*

Fig. 1 Schematic describing the life cycle of plastic materials beginning with human production and use through breakdown and accumulation in food and water sources, ultimately returning to humans. Generated in BioRender; modified from Yee, *et al.*

period *via* pregnancy or lactation.[16] The presence of microplastics in human ovarian follicular fluid was found in 14 of 18 individuals undergoing *in vitro* fertilisation (IVF) fertility treatment.[17] Researchers have confirmed the presence of microplastics in the semen of six of ten individuals living in a polluted area of Southern Italy.[18] PS was confirmed in three of these six individuals. These findings indicate that nanoplastics and microplastics, including PS, are present in reproductive organs and fluids, and therefore may impact fertility and other reproductive-associated health outcomes. Additionally, repeated oral dosing in mice resulted in accumulation of PS NPs that impaired the intestinal barrier.[19] Specifically, polystyrene is used to produce plastic containers, Tupperware, cups, and several other plastic items, which are extremely prevalent in the environment. Generally, we have very little knowledge of the effect that these micro- and nano-plastics will have on the human body.[20]

Cancers of the reproductive system, such as ovarian, testicular, endometrial, and cervical cancers, are often linked to dysfunction in the endocrine system. EDCs are thought to be a cause of endometrial cancer, which is the most common gynaecological malignancy worldwide,[21] and saw a 132% increase in cases from 1990 to 2020.[22] One potential cause for this rising incidence is exposure to EDCs and the subsequent disruption of DNA replication.[23] Additionally, endometrial cancer is associated with Lynch syndrome, which affects 30–40% of individuals diagnosed with endometrial cancer,[24,25] and involves a set of heritable germline mutations in the *MLH1*, *MSH2*, *MSH6*, or *PMS2* genes.

Most women diagnosed with endometrial cancer who have Lynch syndrome are diagnosed at a median age of 48; 15 years earlier than the overall median age of 63 years. In non-cancerous cells, the proteins encoded by these genes are responsible for correcting errors in DNA replication. However, in cancers with gene mutations, these proteins lack proper function to correct mispaired bases, small deletions, or small insertions, leading to the accumulation of mutated cells.[26] In the mussel *Mytulus galloprovincialis*, polystyrene microplastics were confirmed to cause DNA double-strand breaks and suspected to cause reproductive risk.[27]

In the present study, we utilize a CRISPR-modified cervical cancer cell line to investigate the impact of PS nanoplastics on DNA-mismatch repair *via* the *MLH1* and *MSH2* genes.[28] Functionally, MSH2 forms a protein complex with MSH6, and MLH1 forms a protein complex with PMS2; therefore, knockouts of MSH2 and MLH1 are sufficient to inhibit these pathways.[29] We used commercially available polystyrene particles of uniform size as the nanoplastic in this study. These particles were characterized upon receipt for size, shape, composition, and surface charge to enhance the understanding of observed effects on the cells and to confirm manufacturer specifications. We examined the almost immediate (24 hours) effects that PS NPs have on gynaecological cells, focusing on model cervical cancer cells with cancer-promoting mutations in the form of deficient mismatch repair (MMR). The cell viability and oxidative balance of wild-type (WT) HeLa cervical cancer cells, MSH2 knockout (KO) HeLa cervical cancer cells, and MLH1 KO HeLa

cervical cancer cells. Furthermore, we investigated cellular internalization using fluorescent PS (FPS) both quantitatively and qualitatively. These investigations highlight how PS nanoplastics impact the reproductive system, particularly in relation to gene mutations.

Results

The PS NPs and FPS NPs were characterized upon receipt. Attenuated total reflectance Fourier transform infrared spectroscopy (ATR-FTIR) was used to confirm the presence of expected bonds in polystyrene and fluorescent polystyrene (Fig. 2). Polystyrene is formed from the styrene monomer, and the polystyrene nanoparticles contain terminal sulphate groups per manufacturer specifications. In contrast, per manufacturer specifications, the fluorescent polystyrene contains both sulphate and amine end groups. We confirmed the presence of aromatic carbon–hydrogen bonds and carbon–carbon double bonds in both PS and FPS. Further, we confirmed the silicon–oxygen double bond from the sulphate groups in both samples. The bands for primary amines overlap with other bands for the polystyrene backbone and therefore were not observed in this study.

The average diameter of the particles was obtained using SEM and FIJI.[30,31] Both the PS and FPS NPs were spherical and

uniform in size (Fig. 3). The average diameter of the particles was calculated from 500 particles. The average diameter of the PS NPs was 86.61 ± 6.41 nm, and the average diameter of the FPS NPs was 63.34 ± 13.81 nm. Additionally, the FPS had a much larger size distribution compared with the PS, and more particles at each of the tails of the sample distribution compared with the PS.

A water bath sonicator was used to disperse nanoparticles in water, and it was determined that sonication time had no significant impact on particle size distribution over 15-minute increments for 90 minutes (Fig. 4). In contrast, changing the concentration of PS in solution resulted in significant differences between the 1000 μg mL^{-1} concentration and the 500 μg mL^{-1} and 10 μg mL^{-1} concentrations (Table S1). However, after the first dilution from 1000 μg mL^{-1} to 500 μg mL^{-1}, no significant differences were observed among the other concentrations.

The zeta potential was measured in phosphate-buffered saline (PBS) to maintain ionic strength sufficient for assessing the charge. The individual variability within samples was much greater for zeta potential measurements compared with the hydrodynamic diameters. As observed with the hydrodynamic diameter, changing the sonication time did not have any significant impact on the observed zeta potential. In contrast, changing the concentration significantly impacted the zeta potential (Table S1). The zeta potential at the lowest concentration, 1 μg mL^{-1}, was approximately zero, whereas at 1000 μg mL^{-1}, the zeta potential was approximately -40 mV. As concentration decreased, the zeta potential approached zero (Fig. 5).

To investigate the biocompatibility of polystyrene nanoparticles with cells, two viability assays were performed to measure different components of cell function (Fig. 6). The calcein AM assay for esterase activity generally resulted in lower cell viability at the same concentration compared with the MTT assay for mitochondrial activity. There were no significant differences observed in viability as a function of concentration in the wild-type cell line nor the knockout cell lines with MTT. In contrast, significant decreases in cell viability were observed from the calcein AM assay for all HeLa cells.

To further evaluate the potential toxicity of polystyrene nanoparticles, the ratio of glutathione (GSH) to glutathione disulfide (GSSG) was measured (Fig. 7). Particle concentrations were chosen at a calculated monolayer coverage and bilayer coverage in a
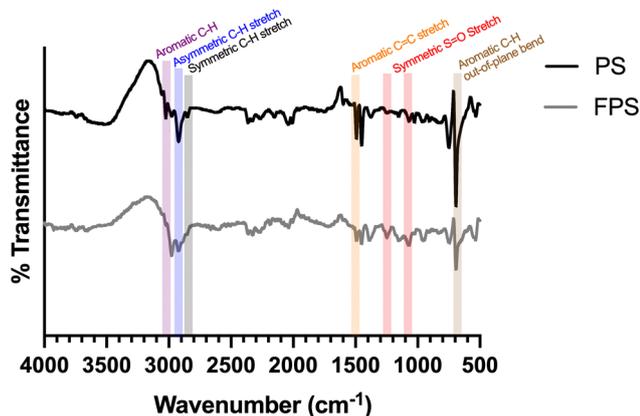

Fig. 2 FTIR characterization of polystyrene (PS) and fluorescent polystyrene (FPS) nanoparticles to confirm the presence of expected functional groups.
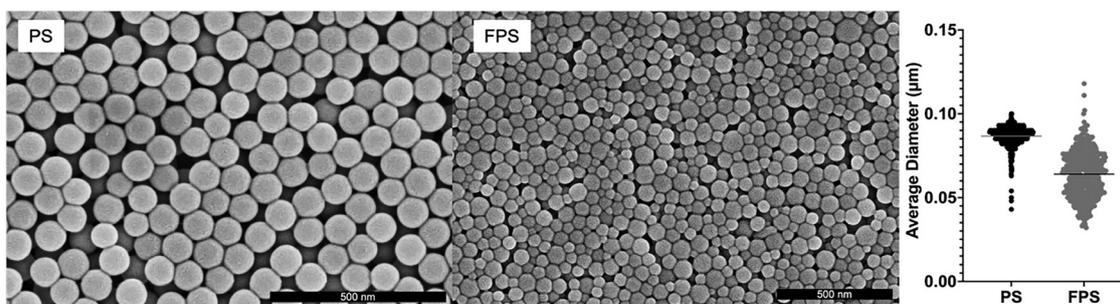

Fig. 3 Scanning electron micrographs (SEM) of polystyrene (left) and fluorescent polystyrene (middle) nanoparticles and size distribution of 500 particles (right). SEM scale bars are equal to 0.5 μm.
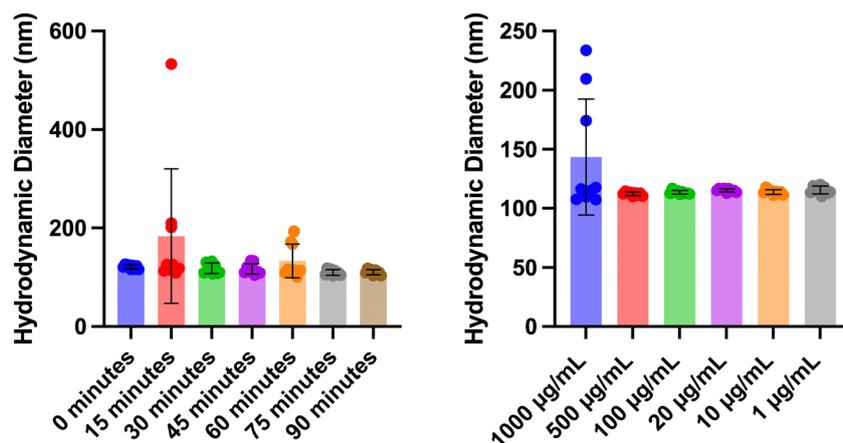
Fig. 4 Hydrodynamic diameter measured *via* dynamic light scattering (DLS) for polystyrene nanoparticles suspended in water as a function of sonication time (left) and concentration (right).
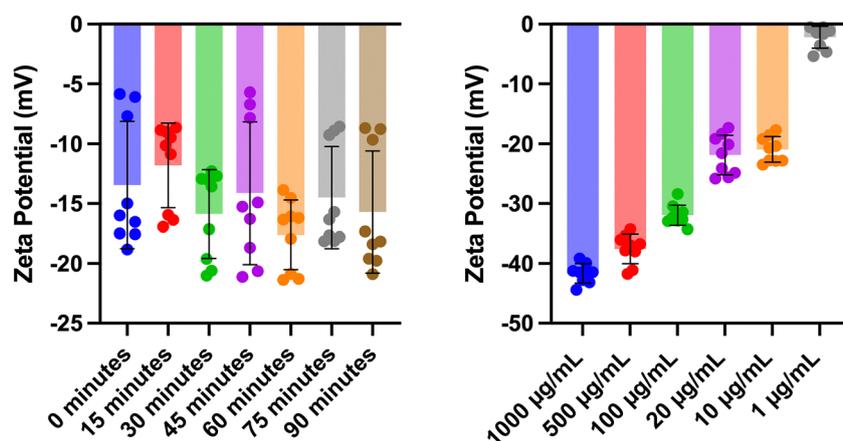

Fig. 5 Zeta potential measured with laser Doppler velocimetry for polystyrene nanoparticles suspended in PBS as a function of sonication time (left) and concentration (right).

96-well plate using the well surface area and the measured diameter of the particles from SEM. After 24 hours of exposure to nanoparticles, the presence of GSH and GSSG was measured and the GSH/GSSG ratio calculated. There were no significant changes in this ratio across concentrations for any of the cell lines.

To confirm and quantify cellular uptake of the polystyrene nanoparticles, we used both a quantitative measure of measuring fluorescence and a qualitative method of confocal microscopy. As the dosed concentration of nanoparticles increased, the observed intracellular fluorescence also increased (Fig. 8). In confocal microscopy, the number of fluorescent particles visible also increased with increasing dose. Notably, nuclear localization was only noticeable at high concentrations in MSH2 knockout HeLa cells, whereas all other doses and cells exhibited cytoplasmic or extracellular localization.

Discussion

Micro- and nano-plastics are a major unresolved pollutant in water sources for human and animal consumption.[13]

Polystyrene (PS) is an amorphous nanoplastic of the bulk materials by the same name. PS has a rich industrial history, first discovered by Goodyear in 1839 and in the 1930s and 1940s was used in production by BASF and The Dow Chemical Company.[32] Today, PS remains in use for consumer goods, including Styrofoam™, packaging, toys, and other daily items.[33] Plastics in the environment take over 500 years to decompose,[34] which also presents unique challenges for investigating nano- and micro-plastic effects in the laboratory. Accelerated degradation or aging of microplastics has been completed sparingly, and requires specialized equipment as reported.[35,36] Even among PS, the PS contaminating the environment has a range of chemical composition, size, shape, and surface properties.[37] These factors highlight a key challenge in microplastic research: establishing a relevant model plastic for the existing studies. In this study, polystyrene latex beads were purchased and characterized upon receipt. The negative charge of the PS NPs was confirmed by zeta potential; however, the FPS NPs exhibited a positive zeta potential likely due to the amine modification, used to facilitate fluorescent conjugation (Fig. S1).
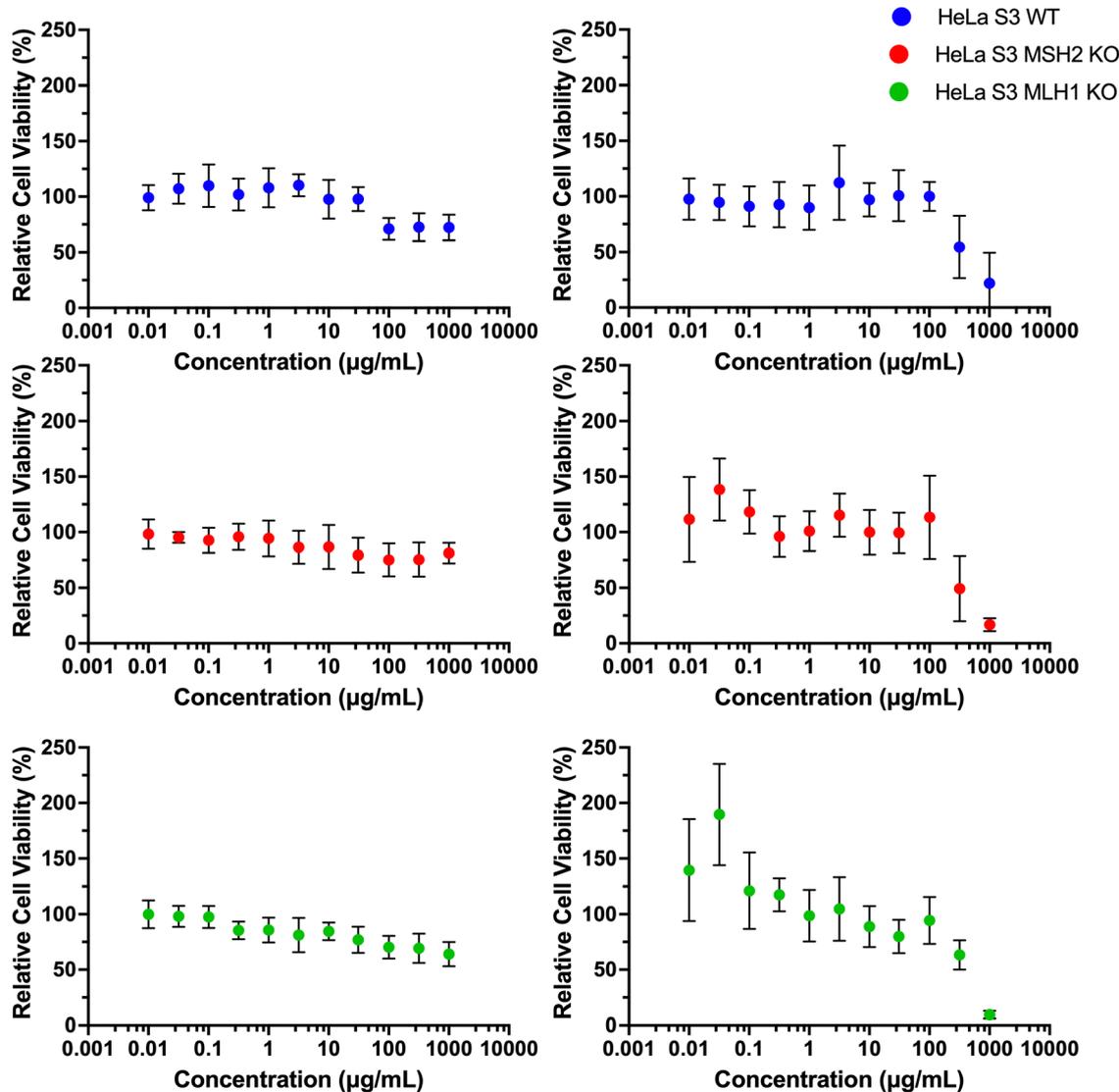
Fig. 6 Relative cell viability using the MTT assay (left) and the Calcein AM assay (right) for HeLa cells, wild-type (top), MSH2 knockout (middle), and MLH1 knockout (bottom).
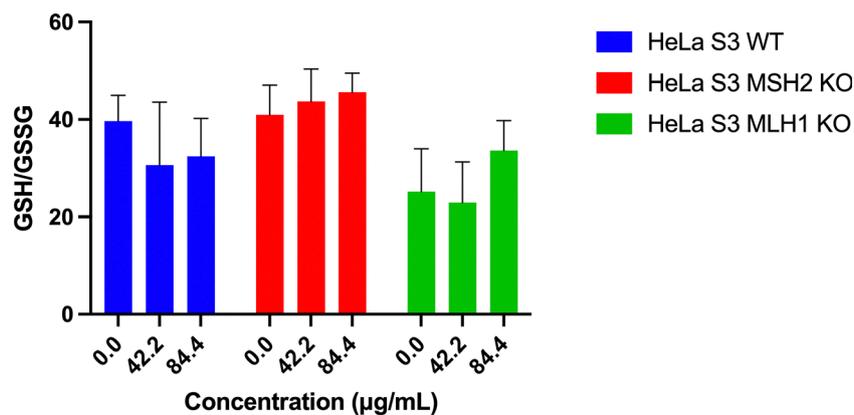

Fig. 7 Ratio of the glutathione balance between GSH and GSSG.

The size of the particles, which was specified as 100 nm, was confirmed using SEM. The particles were also confirmed to have a spherical shape *via* SEM, which is one of the morphological confirmations for microparticles and nanoparticles
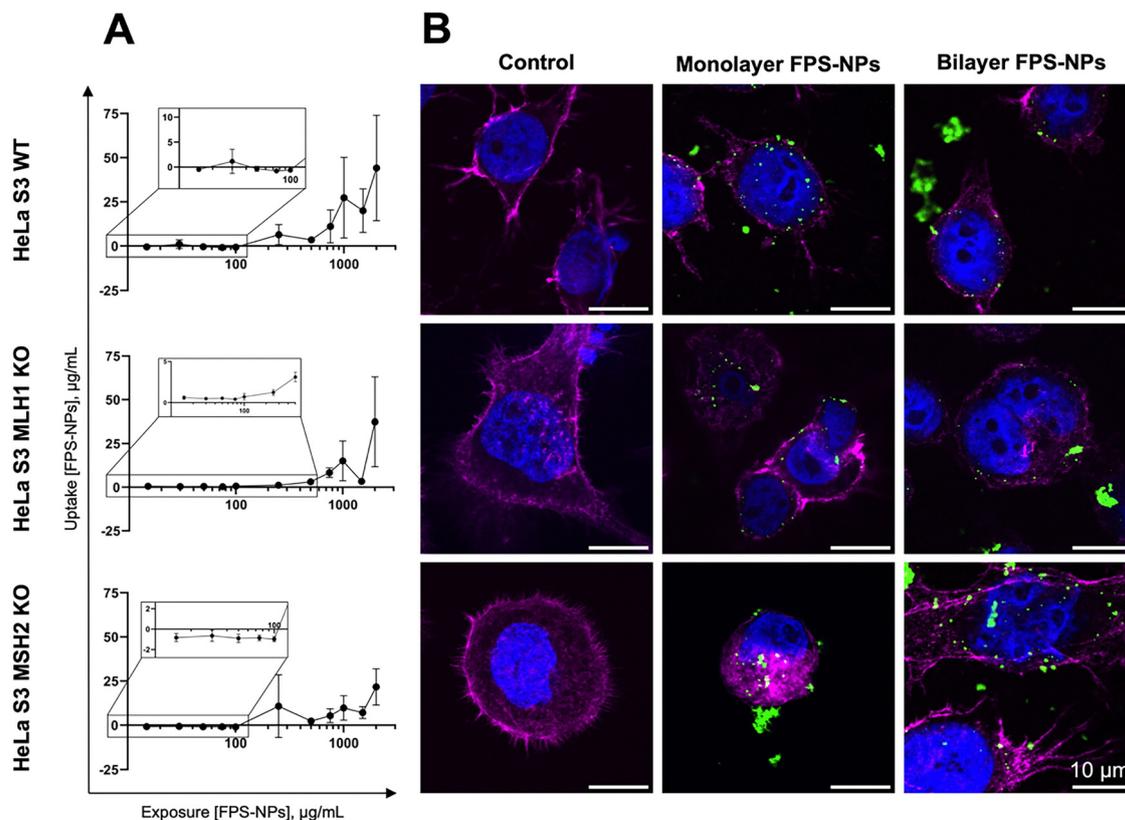
Fig. 8 Particle uptake measured by intracellular fluorescence (A) and confocal microscopy (B). Confocal images represent merged images of single z-layer of HeLa S3 WT, MLH1 KO, and MSH2 KO cell lines following 24-hour treatments with either no particles or mono- (7 μg cm^{-2}) and bilayers (14 μg cm^{-2}) of FPS NPs.

formed from bulk erosion.[38] The FPS had a much larger size distribution compared with the PS (Fig. 3) and more particles at each of the tails of the sample distribution. This may be an effect of the dye conjugation; the FPS particles are prepared using an amine-modified PS, whereas the PS NPs only had sulphate end groups (Fig. 9). In these particles, fluorophores were likely covalently linked to the PS, with residual end groups remaining.[39] The surface functional groups on colloidal particles greatly impact the adsorption behavior.[40] Per manufacturer specifications, differences in end groups account for variations in particle size distribution, especially after modification, which introduces greater experimental variability for the FPS NPs.

The aggregate diameter was also investigated using DLS, and it was determined that changing the concentration had a stronger effect on the aggregation behaviour than sonication time and additional energy. These observations align with the literature in that PS particles have good colloidal stability.[40] This also suggests that spherical nanoplastics have the greatest number of bonded neighbours but the weakest bond strength, indicating that these bonds may be easily formed and broken.[41] The aggregation of particles in solution is dependent on the ionic strength of the solvent; previous investigations indicate that PS NPs are stable in 350 mM sodium chloride (NaCl) solutions and start to aggregate irreversibly at 500 mM NaCl.[11]
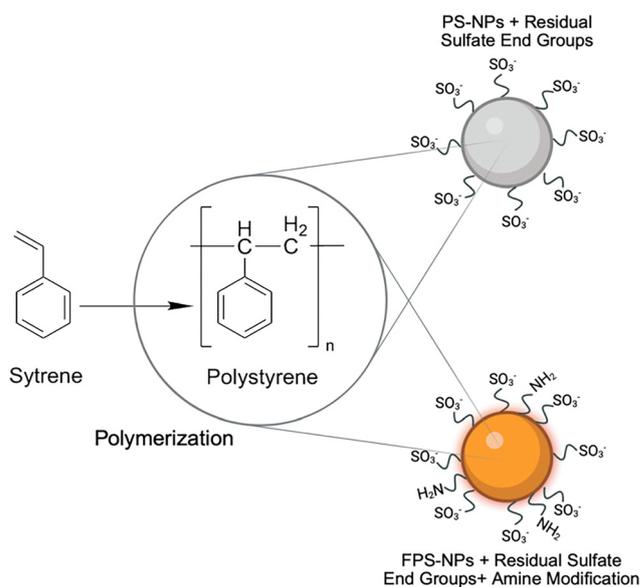

Fig. 9 The schematic shows the synthesis of styrene to generate polystyrene for nanoparticle generation with PS NPs and FPS NPs, both exhibiting characteristic sulfate and amine residual end groups, respectively. FTIR was used to identify the presence of these characteristic sulfate and amine residual end groups and aromatic stretches. Generated in BioRender.

Since the ionic strength of a biologically relevant system is much lower than 350 mM, and rather closer to 50–250 mM at the most concentrated, the aggregation of PS NPs due to ionic interactions is not expected to influence toxicity to humans and human-sourced materials. The zeta potential of unfunctionalised PS approached 0 mV at low concentrations of PS. This indicates that the low concentrations of particles have low colloidal stability and therefore may have a higher tendency towards aggregation. However, the hydrodynamic diameter of these particles remained constant across the different concentrations of PS, indicating that the colloidal stability of these PS particles is not electrostatically driven.[42] Sulphate-modified PS exhibited dispersion in model and natural water via steric hindrance from monatomic cations and aggregation via diatomic cations.[2] The DLVO theory further explain these interactions in colloidal suspensions.[43]

Nanoplastic waste materials pose a significant human health risk due to their small size. Particles from 10–1000 nm are effective for internalization in many cells within the human body and model organisms.[44] Along with endocrine disruption, nanoplastic and microplastics may cause epigenetic modifications to DNA, which result in pathological changes that could lead to cancer development.[45] Specifically, PS NPs were confirmed to disrupt testosterone levels in mice and up-regulated the expression of CYP11A1 and CYP17A1, and 17β-HSD.[46] Importantly, CYP11A1 encodes for cytochrome P450, which is linked to other signalling cascades impacted by PS NP exposure.[47] Despite these findings, the precise mechanisms of these interactions between nano- and micro-plastics and cell membranes which subsequently dominate cell uptake are still under exploration.[48,49] To experimentally assess particle uptake, we qualitatively assessed particle internalisation using confocal microscopy and FPS NPs and confirmed this with quantitative concentrations of fluorescence measured from lysed HeLa cells. Confocal microscopy revealed a dose-dependent relationship between the concentration of particles and their uptake for all cell lines. Specifically, greater PS internalisation was observed for higher doses. However, when assessing the number of particles internalised, results did not show any significant differences in particle uptake compared with an untreated control, below 250 μg mL^{-1}. Additionally, confocal microscopy revealed that particles were localised within the cytosol and cytoskeleton, bound to the cell membrane, and demonstrated the potential for particle accumulation in cells. One potential explanation for this is that 50 nm PS is endocytosed via clathrin- and caveolae-mediated pathways, which begin at the cell membrane and result in the cytosol.[50,51] Furthermore, these results are consistent with prior investigations, particularly one investigation of similarly characterized PS in macrophages, which reported that PS localisation in the cytosol impacted mitochondrial function.[52] The effects of this accumulation were assessed using cell viability. Previous reports indicate that particle uptake is dependent upon both particle size and surface functionalisation. Specifically, aminated particles, such as those used herein, had significantly higher uptake compared with carboxylated or non-functionalised

particles. Therefore, in these studies, the fluorescent particles likely have a greater cell internalisation compared with the unfunctionalised particles.[53] Additionally, using daphnids and 2 μm microplastics, researchers revealed that the carboxyl-functionalised microplastics elicited greater toxicity compared with amine-functionalisation.[54] This uptake is closely linked with the potential toxicity of the cells.

In RAW264.7 cells, PS of 100 nm had no effect on the cell viability; however, amine-functionalised PS induced cell membrane damage, and both amine- and carboxyl-functionalised PS induced mitochondrial-mediated apoptosis.[55] In the present study, the cell viability was assessed using two different assays. The MTT assay specifically measured mitochondrial activity in cells by converting the yellow MTT dye into purple formazan crystals in metabolically active cells. In contrast, the calcein AM assay measured the esterase activity through the conversion of non-fluorescent calcein AM to green, fluorescent calcein via an esterase reaction in the cytoplasm of live cells. The results indicated that esterase activity showed greater declines in cell viability compared to mitochondrial activity. Likewise, in breast cancer cell lines, polystyrene sulfonate particles did not induce cell death.[56] This could be an effect of the localization of the PS to the cytosol as observed in the confocal microscopy imaging, without permeation to the mitochondria. The effects of oxidative stress and oxidation pathways, which integrate with the mitochondria.

The results of this oxidative balance between GSH and GSSG indicated that there was no significant change in glutathione ratios when cells were exposed to 10 or 20 μg mL^{-1} after 24 hours. GSH is a major antioxidant in human cells; as GSH neutralizes excess oxidants, GSSG forms. This biological redox reaction makes the ratio of GSH to GSSG a key indicator of oxidative stress.[57] These data suggest that oxidative stress may not be the mechanism of cell distress in these cell lines. Oxidative stress measured via lipid damage (LPO), catalase activity (CAT), glutathione-S-transferase activity (GST), and GSH of mussel gonad homogenates indicated that PS did not impact GST or GSH, but did impact LPO and CAT.[58] These findings further indicate that oxidative stress can take on many forms, and a single metric may not explain oxidative stress in its entirety. In A549 lung adenocarcinoma cells, amine-functionalised PS nanoparticles of 80 nm elicited greater reactive oxygen species (ROS) compared with non-functionalised PS,[59] therefore the observed levels of oxidative stress are likely the baseline level for PS exposure. In vivo studies with orally administered PS indicated that ROS was produced in excess in the liver,[60] possibly due to first-pass metabolism and high liver accumulation or an effect of liver cell function distinct from cervical cancer cells. Alternative pathways may be the mitophagy pathway or endoplasmic reticulum stress, both of which have been shown to occur following exposure to PS NPs.[61,62] Each of these pathways still impacts mitochondrial damage, which has been confirmed as a mechanism in response to 80 nm PS NPs in non-malignant L02 hepatic cells and BEAS-2B bronchial epithelial cells.[63]

Taken together, these data indicate that the MLH1-deficient HeLa cells exhibited the greatest sensitivity to PS NPs compared

with the WT or the MSH2-deficient HeLa cells. Other literature indicates that MLH1-knockout cells are more sensitive to oxidative stress-inducing agents compared with MLH1-proficient counterparts.[64,65] MLH1 plays a dual role in both mismatch repair and mitochondrial homeostasis as a result of intrinsic dysfunction of mitochondira;[64] therefore, when environmental stressors appear, such as PS NPs, MLH1-deficient cells lack the ability to repair their DNA, and their reduced antioxidant response makes them more sensitive to these pollutants. In renal epithelial cells, researchers confirmed PS-induced mitochondrial dysfunction through oxidative respiration, glycolysis, and glycolytic capacity.[66] A study by Somuncu et al. revealed that a small-molecule drug that targets the mitochondria selectively treated MLH1-deficient colorectal cancers, while minimizing damage to MLH1-proficient cells.[65] Our results suggest that the introduction of PS NPs allows for ROS production in HeLa S3 MLH1 KO cells to remain damaging and not neutralized due to the cells' lack of antioxidant capacity.

Experimental

Materials

Microparticles based on polystyrene (PS NPs), Latex beads, amine-modified polystyrene, fluorescent orange (FPS NPs), $1\times$ Dulbecco's phosphate buffered saline ($1\times$ DPBS or PBS), penicillin–streptomycin (P–S), 0.1% poly-L-lysine solution, bovine serum albumin (BSA), and dimethyl sulfoxide (DMSO), were purchased from Sigma-Aldrich (St. Louis, MO). Roswell Park Memorial Institute 1640 Medium ($1\times$ RPMI-1640), thiazolyl blue tetrazolium bromide (MTT), ethanol (EtOH), Collagen I, rat tail, ProLong™ Diamond Antifade Mountant, AlexaFluor647-Phallodin, eBioscience™ Calcein AM Viability Dye, foetal bovine serum (FBS), and trypsin–EDTA (0.25%) were purchased from Thermo Fisher Scientific (Waltham, MA). GSH/GSSG-Glo™ Assay kit was purchased from Promega (Madison, WI). Isopropanol (IPA) was purchased from VWR (Radnor, PA). Silicon wafers, adhesive transfer tape, SEM pin stub mounts, and Lacey carbon 300 mesh nickel coated TEM grids were all purchased from Ted Pella (Redding, CA). Ultrapure (type 1) DI H_2O (Direct-Q 3UV, Milli-Q, Burlington MA).

Methods

Nanoparticle characterization

The size and morphology of PS NPs and FPS NPs was identified using scanning electron microscopy (SEM). The nanoplastics in solution were dropped onto a wafer mounted on an SEM mount and dried. The mount was then sputter-coated with 2 nm platinum using the Leica ACE 600 carbon/sputter coater. A FEI Helios Nanolab 660 Focused Ion Beam Scanning Electron Microscope (FIB-SEM) was used with a 2 kV accelerating voltage and a 25 pA current to take images of the nanoplastics. The diameters of the PS NPs and FPS NPs were analysed using ImageJ software.[30,31]

Size and zeta potential of PS NPs and FPS NPs were obtained using the Malvern Zetasizer ProBlue (Malvern Panalytical, Westborough, MA). Samples were prepared at the following concentrations: 1000 µg mL^{-1}, 500 µg mL^{-1}, 100 µg mL^{-1}, 20 mg mL^{-1}, 10 µg mL^{-1}, 1 µg mL^{-1}, in both DI H_2O and $1\times$ PBS. Samples of 10 µg mL^{-1} and 20 µg mL^{-1} were sonicated at 15-minute increments from 0 to 90 minutes in both DI H_2O and $1\times$ DPBS. Three unique samples of each concentration and sonication time were analysed. Each sample was measured 3 times.

To assess the characteristic chemical bonds present in the samples to identify the material, Fourier transform infrared spectrometry (FTIR) was used in the sustainability analytics equipment facility (SAEF) at the University of Kentucky. Samples were prepared by directly pipetting 20 µL of manufactured stock solutions or diluting manufactured stock solutions in Milli-Q DI H_2O and placing 20 µL drop on the crystal of a Thermo Fisher Nicolet iS50 FTIR with ATR capabilities. Background FTIR measurements were removed prior to obtaining FTIR data, Milli-Q DI H_2O FTIR spectra was subtracted, and amplification of signal was used prior to data reporting data to visualize peaks more clearly.

Cell maintenance. According to ATCC, HeLa S3 cells are the clonal derivative of the parent HeLa cell line originating from the late Henrietta Lacks, a 31-year-old black female with human cervical adenocarcinoma. ATCC has confirmed that HeLa S3 cells are positive for human papilloma virus (HPV) sequences using PCR. HeLa S3 wild-type (WT), HeLa S3 MLH1 KO, and HeLa S3 MSH2 KO cells were generated by Dr Eva M. Goellner as previously described.[28] These cells were grown in $1\times$ RPMI-1640 containing 10% (v/v) FBS and 1% (v/v) P–S, referred to as supplemented RPMI-1640 from here on. All cells were incubated at 37 °C and 5% CO_2 in the dark. The cells were subcultured in T-75 flasks and passaged at around 90% confluency. Media was replaced every 2 days.

Cell uptake. Cells were seeded at 1.5×10^4 cells per well in a clear 96-well tissue culture-treated plate and allowed to adhere overnight, incubating at 37 °C and 5% CO_2 in the dark. The following day, the media was replaced with 100 µL of phenol- and serum-free RPMI-1640 containing FPS NPs in ascending doses (0–2 mg mL^{-1}) via serial dilutions. After 24 hours of exposure, the particle solution was removed, and cells were washed three times with $1\times$ DPBS to remove unbound and non-internalized particles. Cells were then incubated for 30 minutes with 100 µL per well of 0.1% Triton-X solution to lyse cells and release FPS NPs into solution. The solutions were transferred to a black-sided, clear-bottom 96-well plate, and the fluorescence was measured at excitation/emission wavelengths of 475/540 nm using a Synergy H1 microplate reader. Experimentally measured uptake was compared to a linear standard curve for FPS in Triton-X buffer with an upper limit of detection at 125 µg mL^{-1} and a lower limit of detection at 1.19×10^{-4} µg mL^{-1}.

Particle localization was performed using Nikon CSU-W1 SoRa Confocal Spinning Disk Microscope at the Light Microscopy Core at the University of Kentucky. Confocal slides were prepared by first coating 18 mm circular glass coverslips in

500 μL per well of 0.01% PLL in a clear 12-well plate. After 15 minutes, PLL was removed, and wells were washed (500 μL per well) with 1× DPBS to remove any excess PLL. Coverslips were coated with 10 μg cm^{-2} of Rat Tail Collagen and incubated for one hour at room temperature before being washed with 1× DPBS to remove excess collagen. Cells were then seeded at 1.2 × 10^5 cells per well in supplemented RPMI-1640 and allowed to adhere overnight, incubating at 37 °C and 5% CO$_2$. The following day, media was replaced with phenol- and serum-free 1× RPMI-1640 containing FPS NPs in control, mono-, and bilayer densities (0, 7, and 14 μg cm^{-2}, respectively). After FPS NPs were allowed to incubate with cells for 24 hours, cell media and particles were removed. Cells were washed three times with 1× DPBS before being fixed with 500 μL per well of cold (4 °C) 4% paraformaldehyde for 10 minutes. Paraformaldehyde was removed and cells were washed twice with 1× DPBS. Cells were then permeabilized with 500 μL per well of 0.1% Triton-X for 5 minutes and then washed twice with 1× DPBS. To reduce non-specific binding, 500 μL per well of 1% (w/v) BSA/1× DPBS was incubated with cells for one hour and then washed once with 1× DPBS. Cells were stained with 0.165 μM AlexaFluor647-Phalloidin in 1× DPBS for 45 minutes and then washed twice with 1× DPBS. A single drop of ProLong™ Diamond Antifade Mountant with DAPI was used to mount coverslips onto glass microscope slides. The edges were sealed with clear nail polish and slides were allowed to air dry before being refrigerated (4 °C) until imaged. Z-stack images were acquired with an oil-immersion 60× objective at 60 ms exposure and 50% laser power for the blue, green, and far-red channels. For Z-stack images acquired with an oil-immersion 60× objective using the SoRa 4× setting, 300 ms exposure and 75% laser power was used for the blue and far-red channels, while 200 ms exposure and 50% laser power was used for the green channel. All images were analysed in ImageJ at individual Z-stack planes.

Cell viability. For the MTT viability assay, cells were seeded at 1.5 × 10^4 cells per well in a clear 96-well tissue culture treated plate and allowed to adhere overnight incubating at 37 °C and 5% CO$_2$ in the dark. The following day, media was replaced with 100 μL of supplemented RPMI-1640 containing PS NPs in ascending doses (0–10 mg mL^{-1}). The stock aqueous suspension of PS NPs was vortexed before being used to create serial dilutions. After 24 hours of exposure, particle solution was removed, and cells were washed twice with 1× DPBS. MTT solution was prepared at 5 mg mL^{-1} in 1× DPBS and 10 μL of MTT with 100 μL of media added to each well. The cells were incubated for four hours before the MTT-media solution was removed and replaced with 100 μL per well of 10% (v/v) DMSO/IPA solution. Plates were lightly shaken to solubilize dye before being centrifuged at 1000 × g for 10 minutes to remove particle and cell debris. The supernatant (70 μL) was transferred to a new, clear 96-well plate before measuring absorbance using a Synergy H1 microplate reader at 570 nm. Relative cell viability percentage was determined using normalization to the control group.

For the calcein AM assay, cells were seeded at 1.5 × 10^4 cells per well in a clear 96-well tissue culture treated plate and allowed to adhere overnight incubating at 37 °C and 5% CO$_2$ in the dark. The following day, media was removed and replaced with 100 μL of supplemented 1× RPMI-1640 containing PS NPs in ascending doses via serial dilution (0–10 mg mL^{-1}) as well as an empty control column (no cells, just media). After 24 hours of exposure, the particle solution was removed, and cells were washed three times with 1× DPBS, pipetting up/down three times per well on the first wash. Cells were then incubated with 100 μL per well of 1 μM calcein AM in phenol- and FBS-free RPMI-1640 culture media. After 30 minutes, the dye solution was removed, and the cells were incubated in phenol-free, 10% FBS-supplemented RPMI-1640 for 30 minutes to allow for AM ester removal. Cells were then treated with 100 μL of 1× DPBS. Fluorescence was measured at ex/em 490/520 using Synergy H1 microplate reader.

For the GSH/GSSG assay, tissue-cultured, clear-bottom, white-walled 96-well plates were coated with 10 μg cm^{-2} Rat Tail Collagen I for one hour at room temperature to enhance cell attachment. Collagen solution was removed, and plates were washed once with 150 μL of 1× DPBS. Cells were plated at 1.5 × 10^4 cells per well for optimum luminescence measurement and sufficient cell counts. Cells were incubated at 37 °C and 5% CO$_2$ and left to attach overnight. Media was removed, and cells were treated with RPMI-1640 containing FPS NPs in mono- and bilayer densities (7 μg cm^{-2} and 14 μg cm^{-2}) and control well with no FPS NPs. The treatments were performed in triplicate wells for both total glutathione and oxidized glutathione measurements. After 24 hours, media treatments were removed from wells and cells were washed once with 150 μL 1× DPBS. GSH/GSSG Promega kit was followed using manufacture instructions. Background luminescence of no-cell wells with identical protocols for total and oxidized glutathione was removed before data was analysed using luminescence comparisons between total glutathione and oxidized glutathione measurements.

Statistical analysis. The relative cell viability (%) from MTT and calcein AM assays was compared across a single cell line using a one-way ANOVA with Brown–Forsythe and Welch's correction, followed with a Dunnett's T3 multiple comparisons test (*post hoc* test). Statistical significances are defined as $p \geq 0.05$ ns, $p < 0.05$*, $p < 0.001$**, $p < 0.0005$***, and $p < 0.0001$****. One-way ANOVA with Brown–Forsythe and Welch's correction handles the unequal variances in viability results. A two-way ANOVA with Tukey's post-test was used to compare relative cell viability across all three cell lines at a single concentration.

Conclusions and outlook

Our studies indicated that PS nanoplastics (<100 nm) are highly uniform in size, zeta potential, and morphology. In HeLa cells, the MTT and calcein AM assays indicated minimal decreases in cell viability following 24-hour PS exposure at low concentrations. However, at high concentrations, the calcein AM assay indicated significant decreases in relative cell viability. Furthermore, the

oxidative balance between GSH and GSSG at low doses showed no difference. Contextualizing these data with the uptake and localization of FPS indicates that cell uptake is not occurring at low doses and only the MSH2-knockout HeLa cells have intracellular particles at high doses. Together, these data indicate that PS nanoplastics are potentially harmful at high doses. Environmentally relevant concentrations are still under exploration, and it is unclear how many microplastics humans may be exposed to in each day or across the lifespan. To our knowledge, this is the premiere study to explore the effects of model nanoplastics on cervical cancer cell function, specifically CRISPR-modified knockouts associated with the MMR DNA repair pathway associated with Lynch syndrome. Another common plastic, and therefore nano- and micro-plastic, is poly(ethylene terephthalate), PET. Developing PET particles for testing, whether *via* plastic breakdown or PET synthesis, has proven challenging. However, phthalates are also known endocrine disruptors and may have significant impacts on individuals with Lynch syndrome, such as is investigated in this study with CRISPR knockouts. The environmental prevalence of nano- and micro-plastics, and the findings in this study, indicate a need for further investigation on the potential effects of microplastics commonly leached into the environment.

Microplastic accumulation leads to human exposure, and therefore the potential for toxicity to human tissues. Furthermore, highly polluted locations may be co-contaminated with other materials, such as heavy metals, which also have inherent toxicity. Additionally, these materials may interact to result in a combined effect greater than the sum of the parts.[67,68] Subsequent investigations should take care to eliminate potential nanoplastic and microplastic contamination during the experimental process, such as plastics that may leach from popette tips, tissue culture plastic plates, and other sources. Additionally, these studies were conducted using commercially available materials rather than environmentally isolated materials. The ability to isolate materials from contaminated environmental sources is an important future direction for the field of nanoplastic research. Microparticles, including polystyrene, take hundreds of years to degrade, and accelerated degradation techniques have not yet been developed and validated. This drastically limits the current capabilities for researchers to address microplastic and nanoplastic effects on human health in an environmentally-relevant study. Model studies, such as the one presented here, are important to establish testing methods and protocols that can carry through as science continues to advance.

Author contributions

J. D. B., M. C. F., and L. E. M. completed data collection and analysis. B. K., C. E. R., E. M. G., and B. E. G. assisted with data interpretation. J. D. B., M. C. F., and B. E. G. prepared the manuscript for publication. C. E. R., E. M. G., and B. E. G. conceptualized the project.

Conflicts of interest

There are no conflicts of interest to declare.

Data availability

The data tables for these studies are available in the supporting information (SI). Supplementary information is available. See DOI: https://doi.org/10.1039/d5sm01095k.

References

1 R. Geyer, J. R. Jambeck and K. L. Law, *Sci. Adv.*, 2017, **3**, e1700782.
2 J. Wang, X. Zhao, A. Wu, Z. Tang, L. Niu, F. Wu, F. Wang, T. Zhao and Z. Fu, *Environ. Pollut.*, 2021, **268**, 114240.
3 H. Zhang, S. Zhang, Z. Duan and L. Wang, *Environ. Int.*, 2022, **162**, 107177.
4 S. Ghosh, A. Sane, S. Gohil, V. Vashishtha, S. K. Kumar and G. Kumaraswamy, *Soft Matter*, 2025, **21**, 2782–2786.
5 R. Gillibert, A. Magazzù, A. Callegari, D. Bronte-Ciriza, A. Foti, M. G. Donato, O. M. Maragò, G. Volpe, M. L. de La Chapelle and F. Lagarde, *Environ. Sci.: Nano*, 2022, **9**, 145–161.
6 H. Folarin, N. Hajian, K. Hill and A. Laskin, *Soft Matter*, 2025, **21**, 6603–6612.
7 S. Xu, M. Li, Y. Zheng, M. Xu, J. Zhou, S. Wang, S. Li and M. Wang, *Toxicology*, 2025, **516**, 154194.
8 R. Ramasamy and R. B. Subramanian, *Environ. Sci. Pollut. Res. Int.*, 2021, **28**, 41596–41611.
9 L. P. Munoz, A. G. Baez, D. Purchase, H. Jones and H. Garelick, *Environ. Sci.: Nano*, 2022, **9**, 606–620.
10 P. Pontecorvi, S. Ceccarelli, F. Cece, S. Camero, L. V. Lotti, E. Niccolai, G. Nannini, G. Gerini, E. Anastasiadou, E. S. Scialis, E. Romano, M. A. Venneri, A. Amedei, A. Angeloni, F. Megiorni and C. Marchese, *Int. J. Mol. Sci.*, 2023, **24**, 11379.
11 J. Gigault, A. T. Halle, M. Baudrimont, P. Y. Pascal, F. Gauffre, T. L. Phi, H. El Hadri, B. Grassl and S. Reynaud, *Environ. Pollut.*, 2018, **235**, 1030–1034.
12 C. M. Rochman, *Oceanography*, 2020, **33**, 60–70.

13 M. S. Yee, L. W. Hii, C. K. Looi, W. M. Lim, S. F. Wong, Y. Y. Kok, B. K. Tan, C. Y. Wong and C. O. Leong, *Nanomaterials*, 2021, **11**, 496.

14 A. Gonsioroski, V. E. Mourikes and J. A. Flaws, *Int. J. Mol. Sci.*, 2020, 21.

15 M. Singh, N. F. Mendez, M. Valsecchi, G. Kumaraswamy and S. K. Kumar, *Soft Matter*, 2025, **21**, 6023–6033.

16 B. Jeong, J. Y. Baek, J. Koo, S. Park, Y. K. Ryu, K. S. Kim, S. Zhang, C. Chung, R. Dogan, H. S. Choi, D. Um, T. K. Kim, W. S. Lee, J. Jeong, W. H. Shin, J. R. Lee, N. S. Kim and D. Y. Lee, *J. Hazard. Mater.*, 2022, **426**, 127815.

17 L. Montano, S. Raimondo, M. Piscopo, M. Ricciardi, A. Guglielmino, S. Chamayou, R. Gentile, M. Gentile, P. Rapisarda, G. Oliveri Conti, M. Ferrante and O. Motta, *Ecotoxicol. Environ. Saf.*, 2025, **291**, 117868.

18 L. Montano, E. Giorgini, V. Notarstefano, T. Notari, M. Ricciardi, M. Piscopo and O. Motta, *Sci. Total Environ*, 2023, **901**, 165922.

19 B. Liang, Y. Zhong, Y. Huang, X. Lin, J. Liu, L. Lin, M. Hu, J. Jiang, M. Dai, B. Wang, B. Zhang, H. Meng, J. J. J. Lelaka, H. Sui, X. Yang and Z. Huang, *Part. Fibre Toxicol.*, 2021, **18**, 20.

20 B. Jiang, A. E. Kauffman, L. Li, W. McFee, B. Cai, J. Weinstein, J. R. Lead, S. Chatterjee, G. I. Scott and S. Xiao, *Environ. Health Prev. Med.*, 2020, **25**, 29.

21 C. E. Rowlands, A. M. Folberg, Z. K. Beickman, E. J. Devor, K. K. Leslie and B. E. Givens, *Small*, 2024, **20**, e2300096.

22 E. J. Crosbie, S. J. Kitson, J. N. McAlpine, A. Mukhopadhyay, M. E. Powell and N. Singh, *Lancet*, 2022, **399**, 1412–1428.

23 C. Ahn and E. B. Jeung, *Int. J. Mol. Sci.*, 2023, **24**, 5342.

24 I. Modica, R. A. Soslow, D. Black, C. Tornos, N. Kauff and J. Shia, *Am. J. Surg. Pathol.*, 2007, **31**, 744–751.

25 P. Morice, A. Leary, C. Creutzberg, N. Abu-Rustum and E. Darai, *Lancet*, 2016, **387**, 1094–1108.

26 K. Nuuri, Y. Arroyo and M. Esposito, *J. Young Investig.*, 2020, 38–48.

27 C. Marinaro, G. Scarciello, A. R. Bianchi, B. Berman, T. Chianese, R. Scudiero, L. Rosati, A. De Maio, G. Lettieri and M. Piscopo, *Chem.-Biol. Interact.*, 2025, **405**, 111309.

28 A. K. Miller, G. Mao, B. G. Knicely, H. G. Daniels, C. Rahal, C. D. Putnam, R. D. Kolodner and E. M. Goellner, *Front. Cell Dev. Biol.*, 2022, **10**, 843121.

29 A. Petushkov, J. Intra, J. B. Graham, S. C. Larsen and A. K. Salem, *Chem. Res. Toxicol.*, 2009, **22**, 1359–1368.

30 M. D. Abramoff, P. J. Magalhaes and S. J. Ram, *Biophotonics Inter.*, 2004, **11**, 36–42.

31 J. Schindelin, I. Arganda-Carreras, E. Frise, V. Kaynig, M. Longair, T. Pietzsch, S. Preibisch, C. Rueden, S. Saalfeld, B. Schmid, J. Y. Tinevez, D. J. White, V. Hartenstein, K. Eliceiri, P. Tomancak and A. Cardona, *Nat. Methods*, 2012, **9**, 676–682.

32 A. L. Andrady and M. A. Neal, *Philos. Trans. R. Soc., B*, 2009, **364**, 1977–1984.

33 A. Iizuka, A. Mizukoshi, M. Noguchi and A. Yamasaki, *PLoS One*, 2020, **15**, e0239458.

34 F. Jahedi, N. Jaafarzadeh Haghighi Fard and A. Turner, *Environ. Adv.*, 2025, **19**, 100609.

35 C. Tian, J. Lv, W. Zhang, H. Wang, J. Chao, L. Chai and Z. Lin, *Angew. Chem., Int. Ed.*, 2022, **61**, e202206947.

36 L. Barlucchi, G. Biale, J. La Nasa, M. Mattonai, S. Pezzini, A. Corti, V. Castelvetro and F. Modugno, *Sci. Total Environ.*, 2024, **954**, 176832.

37 T. Gouin, R. Ellis-Hutchings, M. Pemberton and B. Wilhelmus, *Part. Fibre Toxicol.*, 2024, **21**, 39.

38 T. Gaillard, M. George, E. Gastaldi, F. Nallet and P. Fabre, *Soft Matter*, 2019, **15**, 8302–8312.

39 P. Debie, J. Van Quathem, I. Hansen, G. Bala, S. Massa, N. Devoogdt, C. Xavier and S. Hernot, *Mol. Pharmaceutics*, 2017, **14**, 1145–1153.

40 I. Kanu, A. Ojha, K. Adams, J. Brooks and M. Subir, *Soft Matter*, 2025, **21**, 6814–6822.

41 B. R. Argun and A. Statt, *Soft Matter*, 2023, **19**, 8081–8090.

42 D. H. Napper, *Ind. Eng. Chem. Prod. Res. Dev.*, 1970, **9**, 467–477.

43 B. E. Givens, E. Wilson and J. Fiegel, *Colloids Surf., B*, 2019, **179**, 374–381.

44 J. K. Patra, G. Das, L. F. Fraceto, E. V. R. Campos, M. D. P. Rodriguez-Torres, L. S. Acosta-Torres, L. A. Diaz-Torres, R. Grillo, M. K. Swamy, S. Sharma, S. Habtemariam and H.-S. Shin, *J. Nanobiotechnol.*, 2018, 16.

45 G. Rana, A. Donizetti, G. Virelli, M. Piscopo, E. Viggiano, B. De Luca and L. Fucci, *Brain Res.*, 2012, **1467**, 113–119.

46 Y.-Y. Lu, R. Yang, M. Cao, L. Lu, W. Zhu, W. Hua, M. Tian, Y. Sun and Q. Huang, *Environ. Pollut.*, 2025, **366**, 125506.

47 H. Wu, Q. Liu, N. Yang and S. Xu, *Sci. Total Environ.*, 2023, **871**, 161962.

48 A. Azadbakht and D. J. Kraft, *Soft Matter*, 2025, **21**, 4730–4738.

49 D. A. Redwan, J. Reicher and X. Yong, *Soft Matter*, 2025, **21**, 7420–7432.

50 L. Liu, K. Xu, B. Zhang, Y. Ye, Q. Zhang and W. Jiang, *Sci. Total Environ.*, 2021, **779**, 146523.

51 D. Manzanares and V. Cena, *Pharmaceutics*, 2020, **12**, 371.

52 J. Hwang, D. Choi, S. Han, S. Y. Jung, J. Choi and J. Hong, *Sci. Rep.*, 2020, **10**, 7391.

53 A. Banerjee, L. O. Billey and W. L. Shelver, *PLoS One*, 2021, **16**, e0260803.

54 K. Panagiotidis, B. Engelmann, M. Krauss, U. E. Rolle-Kampczyk, R. Altenburger, K. D. Rochfort and K. Grintzalis, *J. Hazard. Mater.*, 2023, **458**, 132023.

55 J. Chen, Z. Xu, Y. Liu, A. Mei, X. Wang and Q. Shi, *Ecotoxicol. Environ. Saf.*, 2023, **252**, 114574.

56 A. B. Caliari, R. N. Bicev, C. C. da Silva, S. E. G. de Souza, M. G. da Silva, L. E. A. Souza, L. R. de Mello, I. W. Hamley, G. Motta, J. Degrouard, G. Tresset, A. J. C. Quaresma, C. R. Nakaie and E. R. da Silva, *Soft Matter*, 2024, **20**, 9597–9613.

57 X. Gong, X. Pu, J. Wang, L. Yang, Y. Cui, L. Li, X. Sun, J. Liu, J. Bai and Y. Wang, *Int. J. Nanomed.*, 2021, **16**, 6661–6679.

58 T. Chianese, M. Galati, T. Cappello, M. Maisano, G. Lettieri, C. Marinaro, M. Piscopo, G. Fasciolo, C. Gravato and G. Napolitano, *Environ. Toxicol.*, 2025, 1–16.

59 X. Shi, X. Wang, R. Huang, C. Tang, C. Hu, P. Ning and F. Wang, *Int. J. Nanomed.*, 2022, **17**, 4509–4523.

60 X. Fan, X. Wei, H. Hu, B. Zhang, D. Yang, H. Du, R. Zhu, X. Sun, Y. Oh and N. Gu, *Chemosphere*, 2022, **288**, 132607.

61 Y. Huang, B. Liang, Z. Li, Y. Zhong, B. Wang, B. Zhang, J. Du, R. Ye, H. Xian, W. Min, X. Yan, Y. Deng, Y. Feng, R. Bai, B. Fan, X. Yang and Z. Huang, *Part. Fibre Toxicol.*, 2023, **20**, 44.

62 L. G. Pan, D. K. Yu, Y. Zhang, C. Y. Zhu, Q. N. Yin, Y. Hu, X. Q. Zhang, R. M. Yue and X. Xiong, *Sci. Total Environ.*, 2021, **781**, 146753.

63 S. Lin, H. Zhang, C. Wang, X. L. Su, Y. Song, P. Wu, Z. Yang, M. H. Wong, Z. Cai and C. Zheng, *Environ. Sci. Technol.*, 2022, **56**, 12483–12493.

64 S. Rashid, M. O. Freitas, D. Cucchi, G. Bridge, Z. Yao, L. Gay, M. Williams, J. Wang, N. Suraweera, A. Silver, S. A. C. McDonald, C. Chelala, G. Szabadkai and S. A. Martin, *Cell Death Dis.*, 2019, **10**, 795.

65 B. Somuncu, A. Ekmekcioglu, F. M. Antmen, T. Ertuzun, E. Deniz, N. Keskin, J. Park, I. E. Yazici, B. Simsek, B. Erman, W. Yin, B. Erman and M. Muftuoglu, *PLoS One*, 2022, **17**, e0268391.

66 H. Wang, X. Shi, Y. Gao, X. Zhang, H. Zhao, L. Wang, X. Zhang and R. Chen, *Environ. Int.*, 2022, **166**, 107349.

67 S. Liu, J. Shi, J. Wang, Y. Dai, H. Li, J. Li, X. Liu, X. Chen, Z. Wang and P. Zhang, *Front. Microbiol.*, 2021, **12**, 652520.

68 A. Devi, Y. S. K. De Silva, L. Tyagi and Aaryashree, *Microplastics*, 2025, **4**, 38.